Absolute partial and total electron-impact-ionization cross sections for CF_4 from threshold up to 500 eV

Ce Ma, M. R. Bruce, and R. A. Bonham
Department of Chemistry, Indiana University, Bloomington, Indiana 47405
(Received 3 December 1990; revised manuscript received 29 April 1991)

Electron-impact dissociative ionization of tetrafluoromethane (CF_4) was studied with the use of a pulsed electron beam time-of-flight apparatus. The absolute partial ionization cross sections of CF_3^+, CF_2^+, CF_3^{2+}, CF^+, CF_2^{2+}, F^+, and C^+ were measured from threshold up to 500 eV. The total ionization cross section was obtained by charge weighted summing of all the observed partial ionization cross sections. A total cross section for dissociation into neutral fragments was inferred from our total ionization cross section and the total dissociation cross section of Winters and Inokuti [Phys. Rev. A **25**, 1420 (1982)]. The present results for the partial ionization cross sections are as much as 9% (CF_3^+) to 81% (F^+) higher than the previously published absolute measurements of Stephan, Deutsch, and Märk [J. Chem. Phys. **83**, 5712 (1985)] at 80 eV, but are in agreement with their recently revised estimates for the singly charged ions. We also found that dissociative ionization was a dominant process for electron-impact energies above 30 eV, accounting for 85% of the total dissociation cross section at 80 eV.

I. INTRODUCTION

CF_4 has been widely used in the semiconductor industry as a plasma etching gas. The neutral and ionic fragments of CF_4, generated in the low-temperature plasma by low-energy electron (10^0-10^2 eV) impact, play an important role in dry plasma etching of silicon and silicon compounds. To understand and model the plasma etching process using CF_4, one needs to know all types of electron-impact cross sections. Especially important are the partial ionization and neutral dissociation cross sections. However, only one absolute partial ionization cross-section measurement has been reported and that only from threshold to 180 eV [1]. No neutral dissociation cross sections have been reported so far. In the work of Stephan *et al.* [1] an ion beam-deflection technique and a double focusing mass spectrometer were used, the absolute scale was established by normalizing to the Ar^+ partial ionization cross sections. Slavik *et al.* have published relative dissociative ionization curves for CF_3^+ and CF_2^+ from 3 to 150 eV [2].

In the present work we report the absolute partial ionization cross sections for CF_3^+, CF_2^+, CF_3^{2+}, CF^+, CF_2^{2+}, F^+, and C^+ by electron impact on CF_4 from threshold to 500 eV. The total ionization cross section was obtained from the charged weighted sum of the partial ionization cross sections. The total neutral dissociation cross section was inferred from our total ionization cross-section data and the total dissociation cross-section data of Winters and Inokuti [3].

II. EXPERIMENT

A detailed description of the apparatus, the experimental procedure, and the method of absolute scale determination has been given elsewhere [4]. The experimental apparatus employs both crossed pulsed electron-beam–gas-beam and pulsed electron-beam–constant-target gas pressure arrangements in conjunction with a time-of-flight (TOF) mass spectrometer as shown in Fig. 1. Briefly, a pulsed electron beam was obtained by pulsing the control grid of the electron gun. The average electron current measured in the pulsed mode was in the $10^{-13}-10^{-12}$ A range. A typical electron pulse duration was 42 nsec and the experimental repetition rate was about 30 kHz. The electron-beam energy was calibrated with both low-energy elastically scattered electrons and the appearance potentials of Ar^+ and Ar^{2+}. The electron-beam intensity was monitored by a 1-m long Faraday trap [5]. The CF_4 used was purchased from Air Products Co. and the manufacturers stated purity of 99.95% was assumed. After an adjustable period of 10–50 nsec, during which time the extraction field was shorted to ground and the electron pulse was passed through the scattering region, ion extraction was initiated. The extraction field established between the two 40-mm-diam gold screens (91.7% measured optical transmission) separated by 12 mm was typically 8 kV/m. The extracted ions were further accelerated in a 150-mm-long, 60-mm i.d. TOF drift tube, maintained at a constant dc voltage of 300–1000 V, and detected after a final acceleration to 2.25–3 kV by a microchannel plate (MCP) detector. Signals from the MCP were used to stop a LeCroy 4208 real time time-to-digital converter (TDC) with 1-nsec resolution that had been started about 2 μsec after the electron-impact pulse was generated. The time interval between TDC stop and TDC start is directly related to the TOF of the ion within a constant additive factor. By delaying the start of the TDC, the noise pulses generated by switching on and off the ion extraction field can be avoided. The TDC was used in a cascaded mode to allow up to seven hits from a single experiment so that higher count rates could be accommodated without dis-

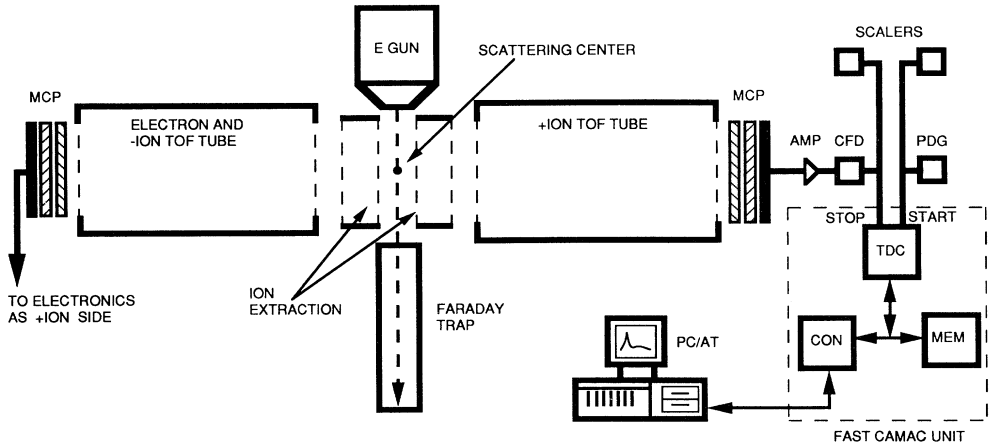

FIG. 1. The pulsed electron-beam time-of-flight apparatus. Acronyms defined as MCP: microchannel plate detector; TOF: time-of-flight; E GUN: electron gun; AMP: preamplifier; CFD: constant fraction discriminator; PDG: pulse delay gate; TDC: time-to-digital converter; MEM: FASTMAC memory; CON: FASTMAC control module.

torting the TOF spectrum. The total ion counts were also monitored by a LeCroy 2551–100 MHz scaler with two channels cascaded for a capacity of 48 bits. The TOF spectra were stored in the memory unit of FASTMAC and transferred to an IBM PC/AT computer every 1–10 min [4].

Beam-beam experiments were carried out to measure the ion count ratios $[CF_2^+:CF_3^+](E)$, $[CF_3^{2+}:CF_3^+](E)$, $[CF^+:CF_3^+](E)$, $[CF_2^{2+}:CF_3^+](E)$, $[F^+:CF_3^+](E)$, and $[C^+:CF_3^+](E)$ as functions of electron-impact energy, E, from threshold to 500 eV. Those experiments took 2–20 h with a statistical accuracy better than 0.5%. Note that the ratios are independent of variations in most experimental parameters with time. A typical TOF spectrum is shown in Fig. 2 for CF_4 at an incident electron energy of 150 eV, 60-V extraction voltage and 300-V drift voltage. The relative partial ionization cross section for CF_3^+ as a function of the electron energy E was also measured by beam-beam experiments but only 1 min was taken for each energy point. As a check on the constancy of experimental conditions, the CF_3^+ ion count rate, $I_{CF_3^+}(E)$, for an electron-impact energy E of 80 eV was recorded before and after the measurement of each new energy

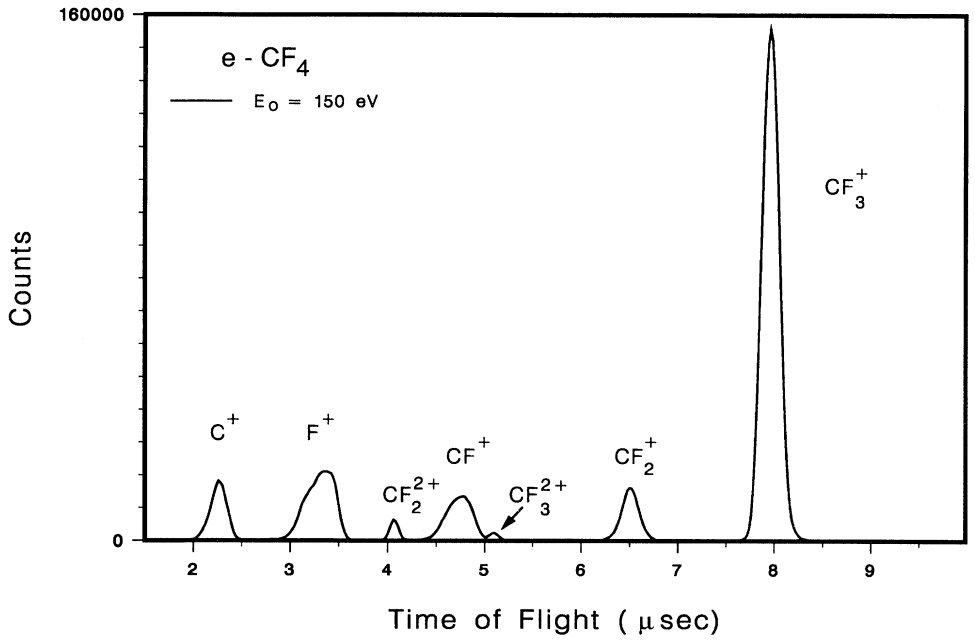

FIG. 2. A typical TOF spectrum using an electron beam and CF_4 gas jet at an electron-impact energy of 150 eV.

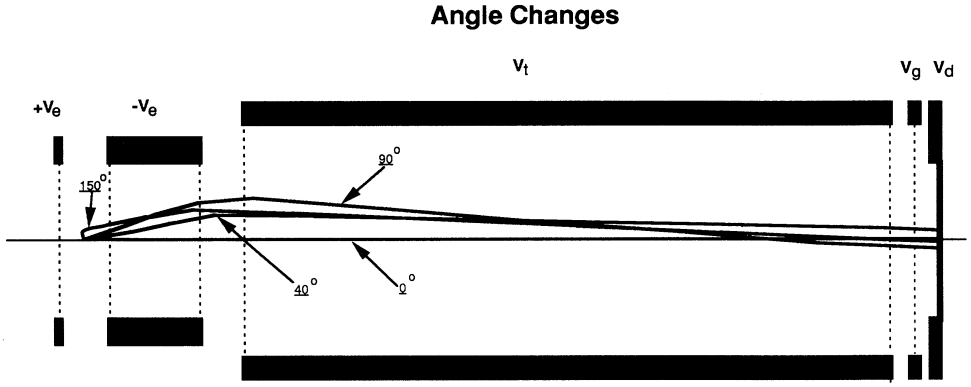

FIG. 3. Ion trajectories from the scattering center to the detector surface with initial angles of 0°, 40°, 90°, and 150°. All ions have the same initial kinetic energy of 10 eV and mass-to-charge ratio of 40 amu. Note that the ion trajectories are mass-charge independent. Experimental conditions are $V_e = 60$ V, $-V_e = -60$ V, $V_t = -1000$ V, $V_g = -1500$ V, and $V_d = -3000$ V.

point. Variations between two 80-eV measurements was always found to be less than 0.7%. The average of the two 80-eV ion currents, with each divided by the average electron-beam current during their 1-min collection period, I_{norm} (80 eV), was then used to define the relative partial ionization cross section $\sigma_{CF_3^+,\text{rel}}$ as

$$\sigma_{CF_3^+,\text{rel}} = [I_{CF_3^+}(E)/I_e]/I_{\text{norm}}(80\text{ eV}) , \quad (1)$$

where E is the electron-impact energy for the point in question, $I_{CF_3^+}(E)$ is the CF_3^+ ion current at the energy E and I_e is the average electron-beam current during the measurements of $I_{CF_3^+}(E)$. The gas-beam intensity variations as inferred from background total pressure, CF_3^+ partial pressure measurements, and pushing pressure measurements were found to change by less than 0.5%, thus no correction was applied.

SIMION [6] calculations were carried out in order to determine the transmission factor for ions of various kinetic energies. In Fig. 3 the trajectories of ions with 10 eV of initial kinetic energy extracted with a potential of 60 V and a drift voltage of 1000 V are displayed as a function of initial direction. In Fig. 4 the ion trajectories for ions with the worst possible ejection angle (90°) are plotted as a function of varying initial kinetic energy using the same lens settings as Fig. 3. These trajectory plots suggest, except for the losses from grid collisions, that 100% of all ions are collected.

The effect due to the finite volume of the scattering region can also be assessed with the aid of Figs. 3 and 4. This is based on the fact that the size of the scattering region between the gas jet and the electron beam is primarily determined by the spatial width of the electron beam, estimated to be 2 mm in diameter. In a worst case scenario, assuming the ions have 10 eV of kinetic energy and are formed by the leading edge of the pulse, the ion will travel in free space until the electric field turns on 5 nsec later. That is to say, under our experimental conditions, a 40-nsec electron-beam pulse followed by a 5-nsec delay prior to extraction, an ion with 10-eV kinetic ener-

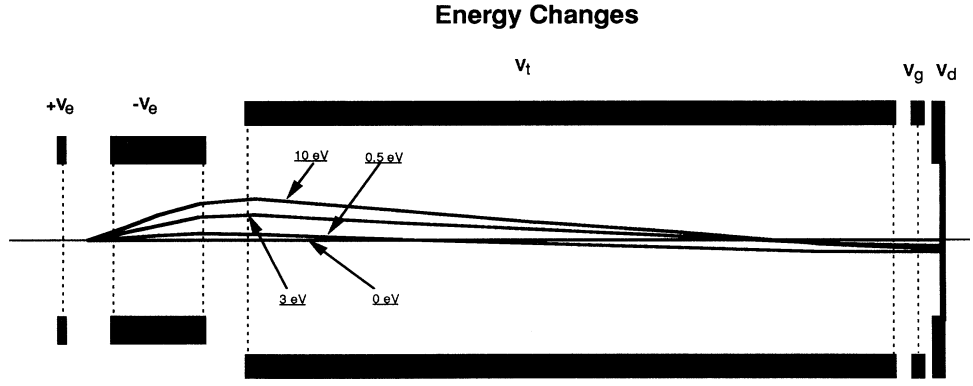

FIG. 4. Ion trajectories from the scattering center to the detector surface with initial kinetic energies of 0, 0.5, 3.0, and 10 eV. All ions have the same initial angle of 90° and mass-to-charge ratio of 40 amu. The experimental conditions are the same as those in Fig. 3.

gy will move 1 mm in 45 nsec. Hence, the diameter of the volume containing the ions when the extraction field is turned on will be less than 3 mm. The maximum effect due to spatial delocalization can be seen in Figs. 3 and 4 by translating the existing ion trajectories vertically 3 mm (one-quarter of the separation distance between the two extraction grids labeled V_e in Figs. 3 and 4).

The relative partial cross section of CF_3^+ was normalized to an absolute scale by pulsed electron-beam–constant-gas-target (transmission) experiments. In this case the entire vacuum chamber was filled with gas by balancing the inlet leak rate against the pumping speed. Gas pressure was measured by using a spinning rotor gauge (SRG) calibrated against absolute capacitance manometers at higher pressures. The measured ion current for CF_3^+ at an incident electron energy E_0 is then given as

$$I_{CF_3^+}(E_0)=\epsilon I_F n l \sigma_{CF_3^+}(E_0) \times \exp\{-n[\langle L\sigma_{\text{ion-mol}}\rangle - L'\sigma_{\text{tot}}(E_0)]\} , \quad (2)$$

where ϵ is the absolute detection efficiency including all losses in the ion transmission optics, I_F is the electron-beam current measured in the Faraday trap during the course of the experiment, n is the number density of the CF_4 gas, l is the path length as viewed by the detector from which ions are extracted, $\sigma_{CF_3^+}(E_0)$ is the sought after absolute cross section for CF_3^+ at an electron impact energy E_0, $\langle L\sigma_{\text{ion-mol}}\rangle$ is the energy-averaged product of the ion flight distance to the detector, L, times the ion-molecule total collision cross section, $\sigma_{\text{ion-mol}}$, L' is the distance from the beginning of the viewing range of the detector to the Faraday trap entrance, and σ_{tot} is the total electron scattering cross section at the electron energy E_0. For our purposes it will be convenient to rewrite Eq. (2) as

$$\ln[Y(E_0)]=\ln(\epsilon l\sigma_{CF_3^+})-n(\langle L\sigma_{\text{ion-mol}}\rangle - L'\sigma_{\text{tot}}) , \quad (3)$$

where

$$Y(E_0)\equiv I_{CF_3^+}/I_F n .$$

By obtaining the total CF_3^+ ion current, $I_{CF_3^+}$, as a function of the gas density n, one can extract the product $\epsilon l\sigma_{CF_3^+}$ from Eq. (3) without knowing the ion-molecule and total electron-scattering cross sections. Figure 5 shows a linear least-squares fit of $\ln[Y(E_0)]$ versus the gas pressure $P=nkT$ for electron-impact energies of $E_0=80$ and 500 eV, where k is the Boltzmann constant and T is the gas temperature in degrees K. The intercepts of the straight lines were found to be 1.398 ± 0.011 and 1.221 ± 0.009 for the electron-impact energies 80 and 500 eV, respectively, where $\sigma_{CF_3^+}$ is in Å^2 and l is in cm.

The detection efficiency ϵ consists of the transmission of the grids and the absolute MCP detector efficiency. The optical transmission of the grid system (five 91.7% optical transmission gold screens) was determined to be $64\pm1\%$ from measuring the attenuation of a light beam passing through the grids. Computer simulation indicat-

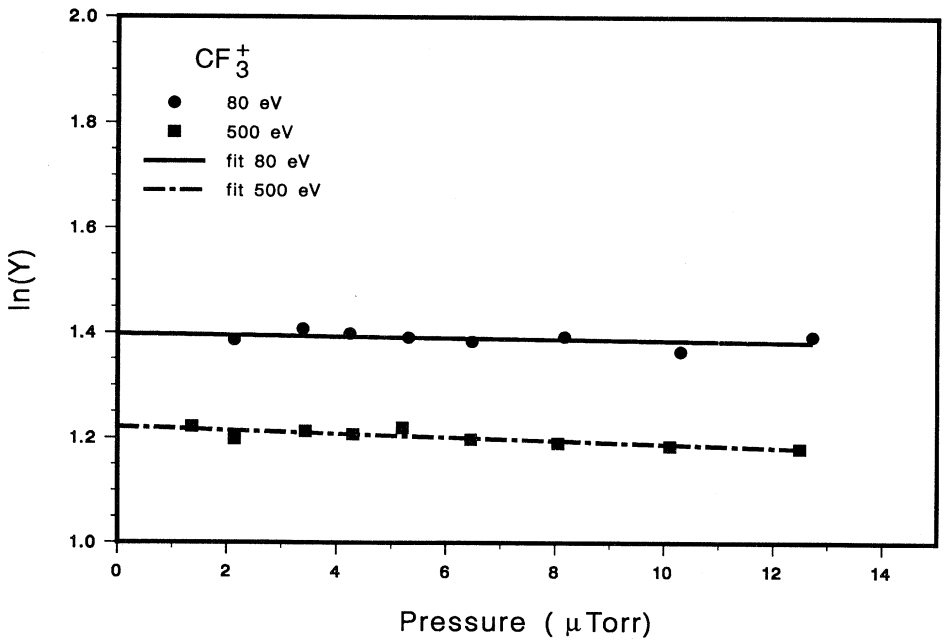

FIG. 5. Linear least-squares fits of $\ln[Y(E_0)]=\ln(I_{CF_3^+}/(I_F n))$ vs CF_4 constant-gas pressure, $P=nkT$ [See Eq. (3)]. Solid and dashed lines: least-squares fits; dots: $E_0=80$ eV; squares: $E_0=500$ eV.

ed that electric-field-induced variations of the transmission from the optical value should be less than 5% [4]. Gao *et al.* found that the detector efficiency was 60% and independent of ion mass or translation kinetic energy above 3 kV for H^+, He^+, and O^+ [7]. Müller *et al.* reported that the detector efficiency for Mg^+ with kinetic energy of 2–3 keV was about 0.6 [8]. Tobita *et al.* reported a value of 0.5±0.1 for 1–10 keV He^+ and 3–10 keV for neutral He [9]. These authors proposed that single-channel efficiencies were 100% for ion energies greater than 1 keV as long as count rates were less than 10^9 cps/m^2. Using the SIMION ion trajectory program [6] we were able to show that positive ions can be detected only if they hit the holes of the MCP and if the potential on the MCP surface is lower than the potential on the screen (V_g in Fig. 3) in front of the detector. By varying the potential between the MCP and the screen, we were able to measure the relative efficiency of the MCP detector as shown in Fig. 6. Note that the efficiency is constant as long as the field draws out secondary electrons away from the front face of the MCP detector and sharply rises by about 34% as the field becomes attractive and the secondaries produced on the front face of the MCP are collected back and presumably focused down the holes. Our picture of the MCP efficiency is that, as long as positive ions are strongly accelerated onto the front face of the MCP, all secondary electrons produced by front-face collisions will go backwards from the plate and the absolute efficiency will just be the ratio of the hole area to the total area of the MCP providing that the ion impact energy is high enough to guarantee that each ion entering a hole has a 100% counting efficiency [9]. We have obtained back-scattering electron microscope images of our MCP's at a resolution of 20 μm/cm and have estimated the efficiency of our plates to be 0.55±0.01 from area measurements. These results are in good agreement with the manufacturers specification of 0.55 for the same ratio. It should be noted that Fig. 6 is essentially identical to the relative efficiency curve for Ar^+ reported in Ref. [4].

The average path length l was calculated from trajectory calculations using SIMION. One-half the effective path length $l/2$ was determined by finding the average value $l/2=[\sum_{i=1}^{6}(r_i^{\max})]/6$, where $r_i^{\max}$ is the largest effective radius along the length of the electron pulse track through the gas at which an ion with one of six ($i=1-6$) initial orthogonal velocities can still reach the detector. The calculation started at $r_i=0$ (the scattering center) and extended to outside of the ion extraction screen until no ions reached the detector. The r_i were incremented in steps of 0.05 mm. In Fig. 7 a plot of the effective path length $l(E_0)$, as a function of the initial ion energy E_0, is

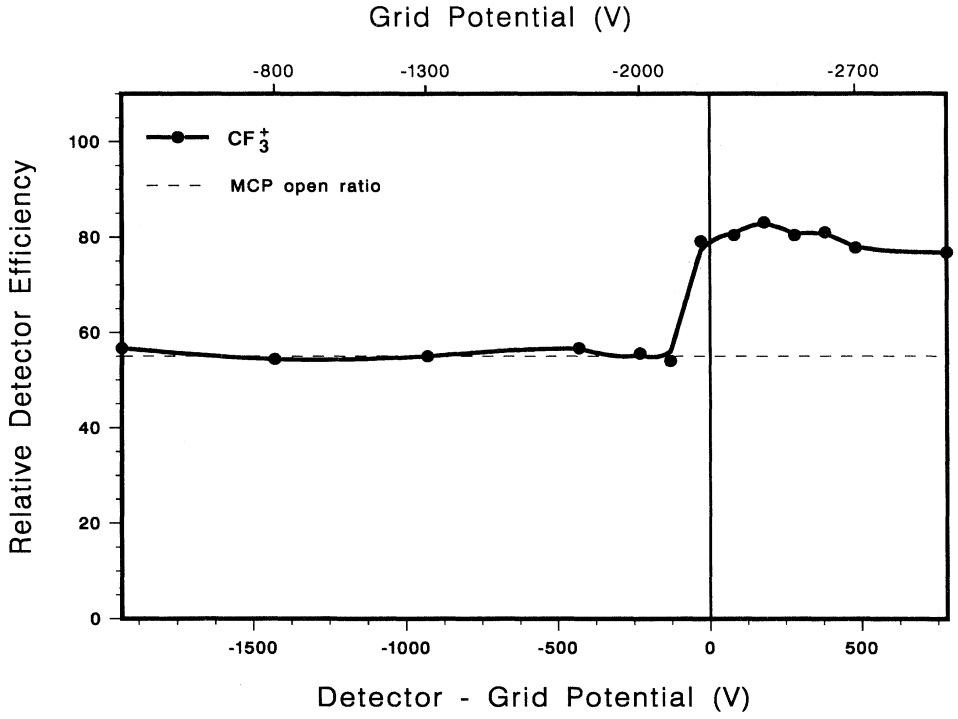

FIG. 6. The relative MCP detector efficiency as a function of the potential difference between the MCP front surface and the nearest grid (V_g in Fig. 3). The voltage scale at the top is the actual potential of the grid while the front surface of the MCP was maintained at a constant value of −2.25 kV. MCP open ratio stands for the ratio of the hole area to the total active area of the MCP.

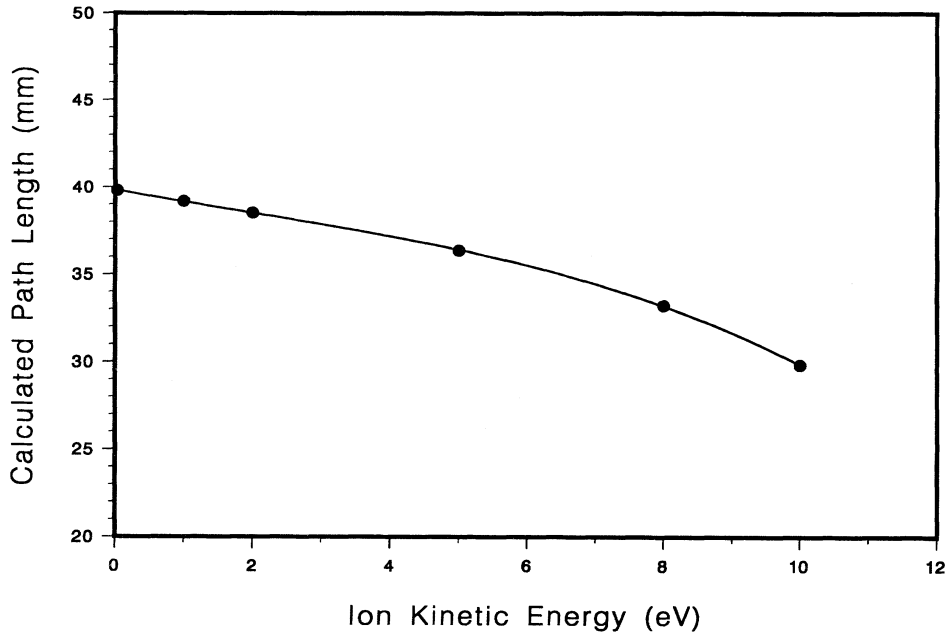

FIG. 7. The calculated scattering length l for the constant-gas target experiment as a function of the initial ion kinetic energy.

shown. Note that $l(E_0)$ decreases as E_0 increases, but the decrease is only 3.4% from room temperature to a translational kinetic energy of 2 eV. This unexpectedly slow decrease is probably due to compensation from trajectories reaching the detector from outside the ion extraction region.

By setting the extraction field to zero, we were able to measure the effective kinetic-energy distribution of CF_3^+ produced at an electron-impact energy of 20 eV as shown in Fig. 8. The kinetic-energy distribution shown in Fig. 8(b) was obtained from the TOF distribution, shown in Fig. 8(a) by direct calculation assuming that each ion traveled 4.9 cm in a field-free region and 15.8 cm in an 800 V drift tube. The results were corrected for different flight paths due to the large detector collection angle (60°). The most probable kinetic energy of CF_3^+ is 1.2 ± 0.5 eV, while the average is about 1.5 eV. This is in agreement with the continuum distribution measured by Brehm *et al.* [10] who found that the most probable energy was between 1 and 1.3 eV (their kinetic-energy distribution decreased in intensity a factor of 2 going from 0.8 to 2 eV). It needs to be emphasized that the ions spend 85% of their flight time in field-free space and that only minor corrections are needed to obtain the velocity distribution. On the other hand, since we are sampling only those ions emitted at $90\pm30°$, we cannot claim that our measured distribution is the average ion energy distribution unless the unknown angular distribution of kinetic fragments turns out to be isotropic.

As a check on the calculation of l, we measured the ion current for CF_3^+ as a function of the extraction voltage from 10 to 80 V for drift voltages of 300 and 800 V. The results are shown in Fig. 9 and indicate the path length $l(E_0)$ to be relatively insensitive to E_0 in this kinetic-

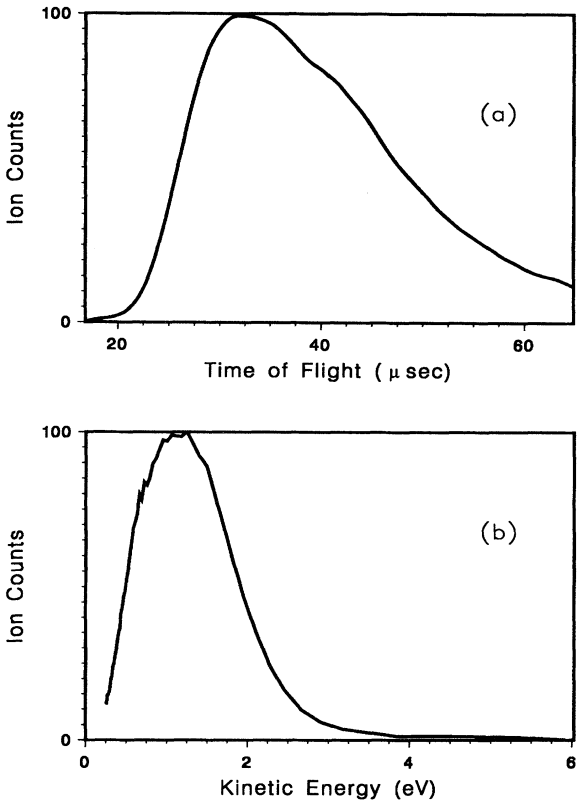

FIG. 8. CF_3^+ ion spectra with no extraction field at an electron-impact energy of 20 eV. (a) TOF spectrum, (b) kinetic-energy distribution of the CF_3^+ ion.

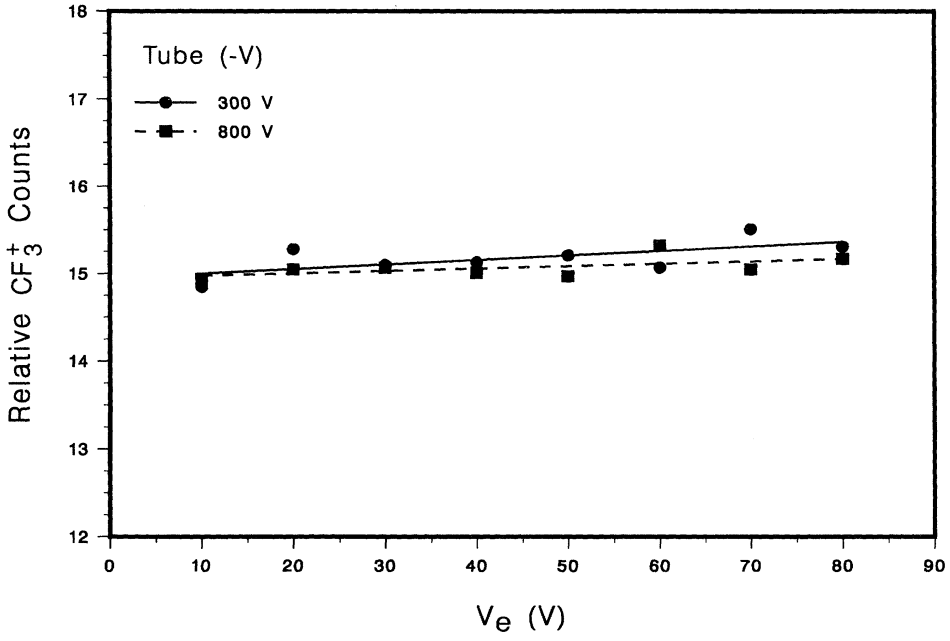

FIG. 9. CF_3^+ ion count rate as a function of the extraction voltage V_e for drift tube potentials of -300 and -800 V.

energy range in keeping with the predictions of theory. The weak link in the constant-gas pressure method of absolute scale determination is in ascertaining l; however, from the evidence just cited, the path length l was taken from Fig. 7 as 3.8 ± 0.2 cm, which is close to the geometric path length 4.0 cm. It should be noted that use of the above procedure to determine the cross section for the much slower Ar^+ ions yielded excellent agreement with results quoted by earlier workers [4].

The relative partial ionization cross sections from a shape measurement can be put on an absolute scale by using the absolute partial ionization cross section of CF_3^+, either $\sigma_{CF_3^+}$ ($E_0=80$ eV) or $\sigma_{CF_3^+}$ ($E_0=500$ eV), as determined from the transmission experiments. The maximum difference between the two normalizations is 4.7%, which is much less than the experimental uncertainties as discussed in Ref. [4]. The average values from the two separately normalized curves were used as the absolute partial cross sections of CF_3^+ reported in this work. The absolute partial ionization cross sections for other lighter-ion fragments were then obtained from the ion ratio experiments and the CF_3^+ cross sections. The total ionization cross section $\sigma_{\rm tot}^{\rm ion}(E)$ of CF_4 for electron-impact energy E from threshold to 500 eV was determined as

$$\sigma_{\rm tot}^{\rm ion}(E)=\sum_i^{\rm all}[q_i\sigma_i(E)]\ , \tag{4}$$

where $\sigma_i(E)$ is the absolute partial ionization cross section, q_i is the number of charges on the corresponding ion fragment, and the sum is over "all" ions produced in the electron-impact ionization of CF_4.

III. RESULTS AND DISCUSSION

In Table I we give the values for the absolute partial ionization cross sections of CF_3^+, CF_2^+, CF_3^{2+}, CF^+, CF_2^{2+}, F^+, and C^+ and the total ionization cross sections $\sigma_{\rm tot}^{\rm ion}(E)$. The uncertainty of these absolute cross sections are about $\pm15\%$. The details of the error analysis are given in Ref. [4]. In the last column of Table I we present the total neutral dissociation cross section for CF_4, with 50% uncertainty, which was obtained by subtracting total ionization cross sections from total dissociation cross sections taken from Ref. [3]. Strictly speaking, the total counting ionization cross section, $\sigma_{\rm count}^{\rm ion}(E)=\sum_i^{\rm all}\sigma_i(E)$, should be used to determine the total neutral dissociation cross section. We estimate from our results that the difference between the total ionization cross section and the total counting ionization cross section is about 2%, hence, the total neutral dissociation cross section may be 14% larger than shown. Note that the results quoted in Ref. [2], which are only relative, were not included in our comparison since the presentation of the data was made by graphs which were reduced in size to the point where it was impossible to obtain accurate values for comparison.

The present total ionization cross sections and total neutral dissociation cross sections for CF_4, as well as the total dissociation cross sections from Ref. [3] and the total ionization cross sections from Ref. [1], are plotted in Fig. 10. Note that the dissociative ionization (at least one product is a positive charged particle) is a dominant process for electron-impact energies above 30 eV, accounting for 85% of the total dissociation cross section at an im-

pact energy of 80 eV.

Electron-impact photon emission studies show strong continuum emission from 200 to 500 nm [11–13] with a measured cross section of 0.65 Å^2 at an electron-impact energy of 100 eV [13]. Becker [14] believes that the excited CF_3^+ ion fragment is the emission source. Wang *et al.* [15] measured the emission spectrum in the range 50–130 nm and showed that the excited fluorine atom was a major emission source in this vacuum uv range, although the observed cross section was only of the order of 10^{-20} cm^2. It seems that ($e+CF_4=CF_3^+ +F+2e$) is a dominant reaction for electron-impact energies above 30 eV. Since dissociation has an appearance potential of 12.5 eV [3], which is lower than the ionization potential of 15 eV, the neutral dissociation process is a dominant process at low-electron-impact energies. The total neutral dissociation cross sections in Fig. 10 exhibit a maximum at low-electron-impact energy and decreases roughly as $1/E$ as the electron-impact energy increases.

As suggested by Fano, the slope of the plot $\sigma E/(4\pi a_0^2 R)$ versus $\ln(E/R)$ gives the square of the dipole matrix element M_n^2 in the Bethe theory [16], where a_0 is the Bohr radius, R is the Rydberg energy, 13.605 eV, E is the electron-impact energy, and σ is the cross section. A Fano plot of the total ionization cross section (TICS) is shown in Fig. 11. A slope, $M_{\text{ion}}^2=20.4$ (in units of a_0^2), was extracted from the higher-electron-energy region (250–500 eV) which is larger than the theoretical Beth asymptote [3] ($M_{\text{tot}}^2=10.3$) but close to the result from the total dissociation cross section (TDCS) of Ref. [3] ($M_{\text{tot}}^2=19.2$). The near-zero slope of the total neutral dissociation cross section in the energy region 180–500 eV might be interpreted as indicating the presence of optically forbidden transitions; however, the large uncertainty in the data (50%) suggests that any such interpretation is, at best, tentative.

Since all electronic excited states of CF_4 and CF_4^+ are unstable [3], the total inelastic cross sections can serve as

TABLE I. Absolute electron-impact ionization and total neutral dissociation cross sections for CF_4 in units of Å^2. Total: the total ionization cross section, $\sigma_{\text{tot}}^{\text{ion}}(E)$; neutral: the total neutral dissociation cross section.

E (eV)	CF_3^+	CF_2^+	CF_3^{2+}	CF^+	CF_2^{2+}	F^+	C^+	Total	Neutral
20	0.365	0.000						0.365	0.449
25	0.884	0.033						0.916	0.770
30	1.468	0.111		0.006				1.584	0.916
35	1.941	0.159		0.044		0.001	0.004	2.148	0.925
40	2.263	0.171		0.107		0.020	0.034	2.595	0.905
45	2.504	0.198	0.002	0.171	0.002	0.057	0.087	3.025	0.891
50	2.695	0.223	0.004	0.202	0.006	0.100	0.124	3.366	0.934
55	2.840	0.242	0.006	0.219	0.011	0.128	0.140	3.601	1.007
60	2.947	0.263	0.011	0.264	0.022	0.212	0.181	3.935	0.908
65	3.027	0.280	0.017	0.303	0.034	0.289	0.216	4.217	0.803
70	3.089	0.293	0.020	0.323	0.040	0.330	0.233	4.387	0.767
75	3.134	0.302	0.022	0.331	0.043	0.351	0.238	4.487	0.775
80	3.167	0.309	0.023	0.334	0.046	0.365	0.241	4.554	0.796
85	3.190	0.314	0.025	0.341	0.048	0.387	0.248	4.626	0.795
90	3.206	0.318	0.026	0.350	0.052	0.415	0.259	4.703	0.774
95	3.215	0.320	0.027	0.360	0.056	0.445	0.269	4.776	0.743
100	3.220	0.322	0.028	0.370	0.059	0.471	0.278	4.833	0.718
110	3.218	0.324	0.028	0.381	0.061	0.501	0.280	4.884	0.701
120	3.206	0.323	0.029	0.384	0.063	0.516	0.277	4.890	0.701
130	3.187	0.322	0.030	0.380	0.064	0.536	0.281	4.893	0.681
140	3.163	0.320	0.032	0.374	0.065	0.556	0.289	4.897	0.649
150	3.137	0.318	0.033	0.368	0.066	0.572	0.295	4.889	0.621
160	3.110	0.318	0.033	0.367	0.066	0.576	0.295	4.863	0.612
170	3.082	0.317	0.032	0.366	0.065	0.573	0.291	4.823	0.618
180	3.053	0.314	0.032	0.363	0.064	0.568	0.287	4.776	0.629
200	2.996	0.302	0.033	0.350	0.062	0.556	0.282	4.675	0.645
225	2.927	0.292	0.030	0.338	0.060	0.539	0.270	4.545	0.634
250	2.862	0.285	0.030	0.323	0.058	0.520	0.261	4.427	0.593
275	2.803	0.278	0.027	0.313	0.055	0.505	0.255	4.319	0.547
300	2.747	0.272	0.025	0.303	0.053	0.485	0.246	4.209	0.511
350	2.649	0.259	0.022	0.280	0.049	0.448	0.229	4.007	0.443
400	2.564	0.248	0.020	0.263	0.045	0.418	0.214	3.837	0.363
450	2.491	0.240	0.019	0.246	0.042	0.395	0.204	3.697	0.283
500	2.427	0.234	0.018	0.233	0.039	0.373	0.194	3.576	0.204

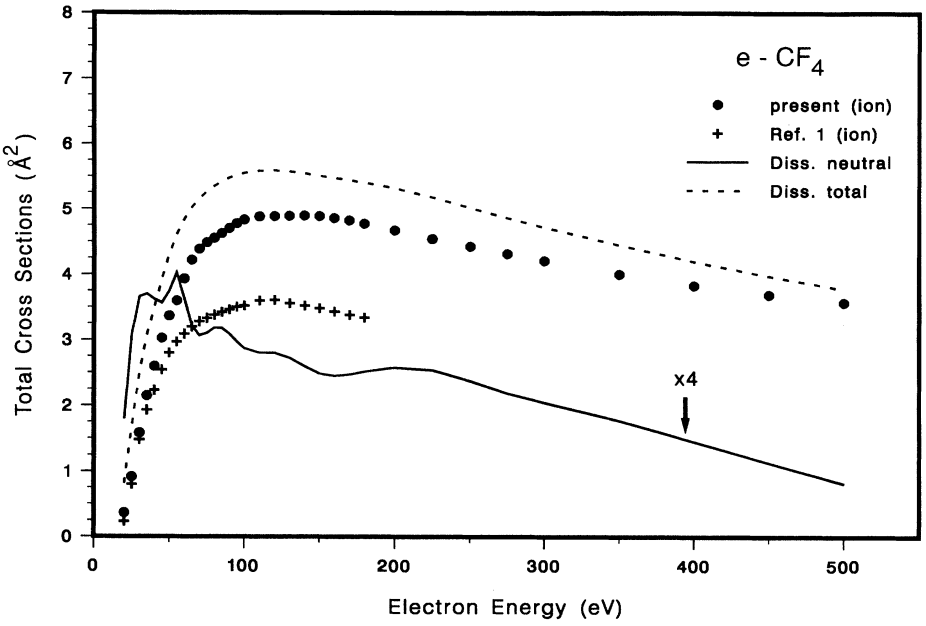

FIG. 10. Total cross sections of CF_4 as functions of electron-impact energy in units of $Å^2$. Dots: present total ionization cross sections; pulses: total ionization cross sections from Ref. [1]; dashed line: total dissociation cross sections from Ref. [3]; solid line: present estimate of the total neutral dissociation cross section.

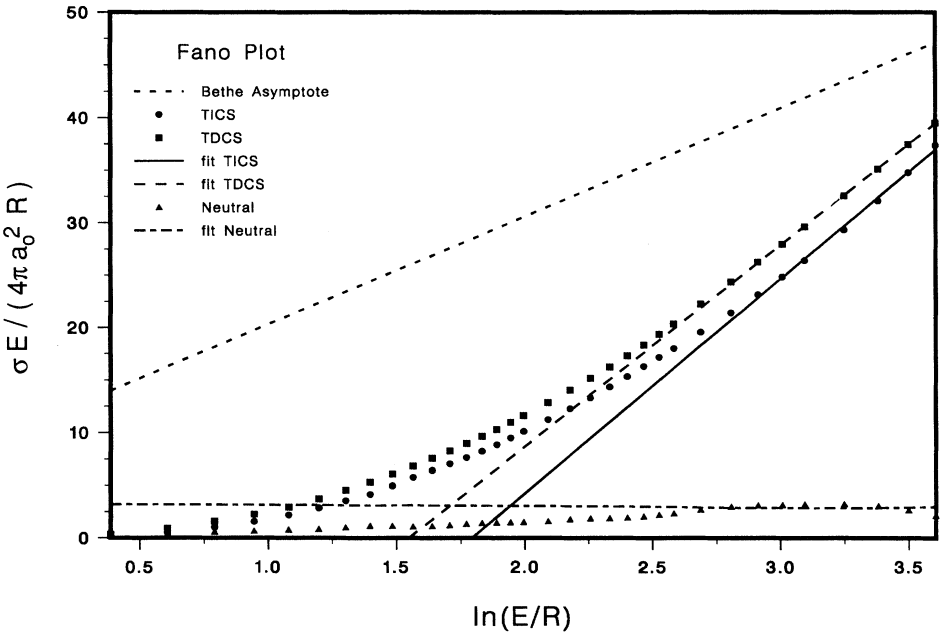

FIG. 11. Fano plot. E is the electron-impact energy, R is the Rydberg constant, σ is the cross section, while a_0 is the Bohr radius. Note that the quantities of both axes are unitless. Other definitions: TICS: the total ionization cross section; TDCS: the total dissociation cross section (Ref. [3]); neutral: the total neutral dissociation cross section; Bethe asymptote: the Bethe theory from Ref. [3] with slope of 10.3. All linear least-squares fits of the TICS and TDCS were performed in the energy region 250–500 eV, and fit for the neutral was done in the energy region 180–500 eV. The slopes for the TICS, TDCS, and neutral curves are 20.4, 19.2, and −0.12, respectively.

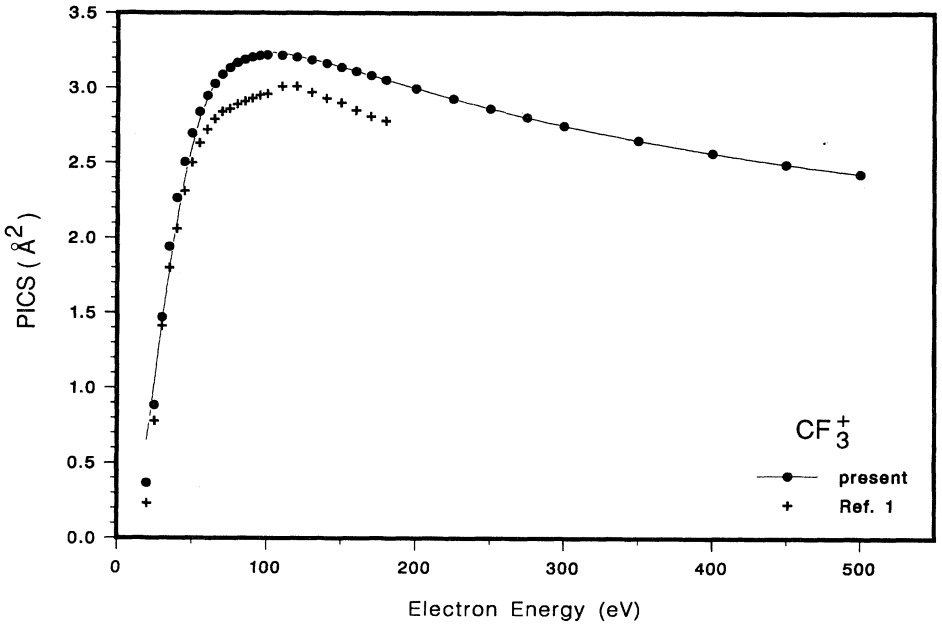

FIG. 12. Absolute partial ionization cross sections (PICS) of CF_3^+. Dots: present work; pluses: Ref. [1].

an upper bound for our total ionization cross sections. The total electron-impact cross section of CF_4 at 500 eV from this laboratory [17] is about 10±2 Å^2. The total electron-impact elastic cross section of CF_4 at 500 eV was calculated to be 5.2 Å^2 by use of the independent atom model (IAM) [18]. The atomic-scattering phase shifts used in the calculation were obtained from Fink [19]. Two sets of absolute experimental data for the angular-dependent electron elastic scattering from CF_4 at 500 eV [20,21] are available. Reference [20] yields a value for the total elastic cross section of 4.68±0.09 Å^2; however, by combining the more accurate small-angle data of Ref.

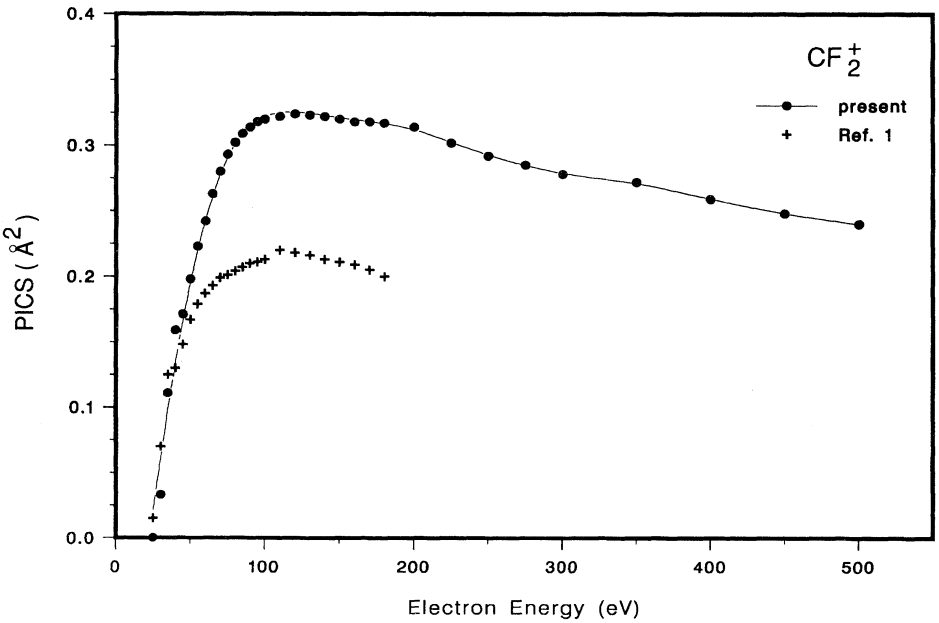

FIG. 13. Absolute partial ionization cross sections of CF_2^+. Dots: present work; pluses: Ref. [1].

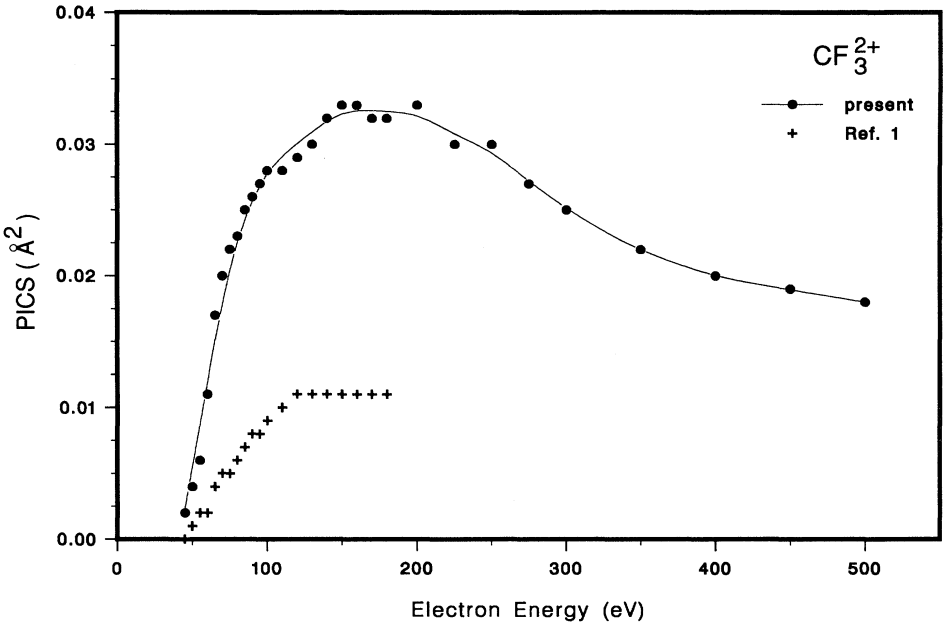

FIG. 14. Absolute partial ionization cross sections of CF_3^{2+}. Dots: present work; pluses: Ref. [1].

[21] with the large-angle data of Ref. [20], a value of 4.46±0.13 Å^2 can be estimated. If we take the latter value as our most accurate estimate (4.5±0.1 Å^2), then a value of 5.5±2 Å^2 is obtained for the total dissociation cross section which compares favorably with the value of 3.8±0.6 Å^2 obtained by the authors of Ref. [3]. The principle source of error in our experiments comes from trying to estimate the total cross section from Jones' data which were taken without the benefit of a monochromater in front of the Faraday trap to eliminate forward scattering.

Our total ionization cross section is much larger than that of Ref. [1] as shown in Fig. 10. At an electron-impact energy of 80 eV, for example, our result is as

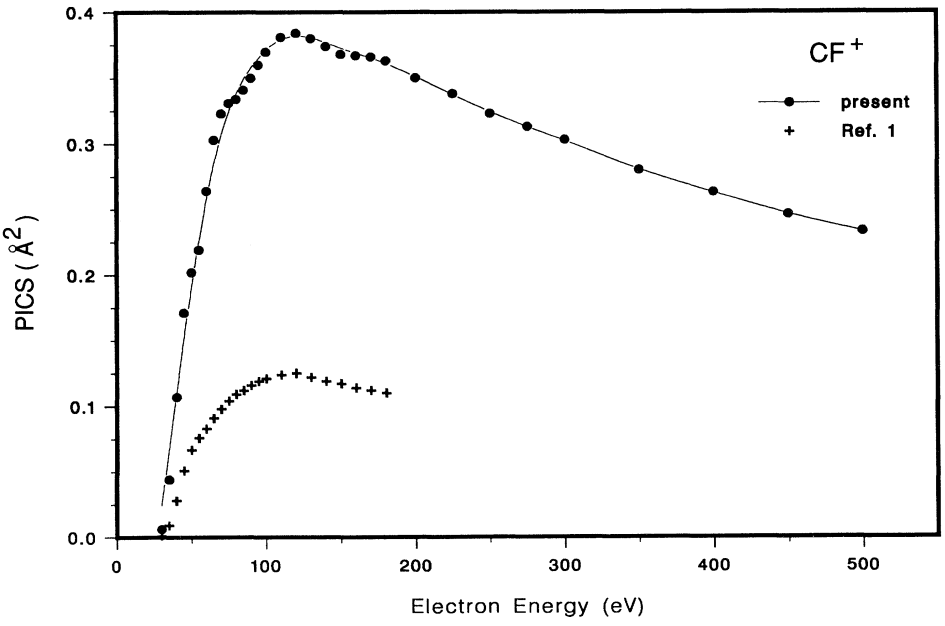

FIG. 15. Absolute partial ionization cross sections of CF^+. Dots: present work; pluses: Ref. [1].

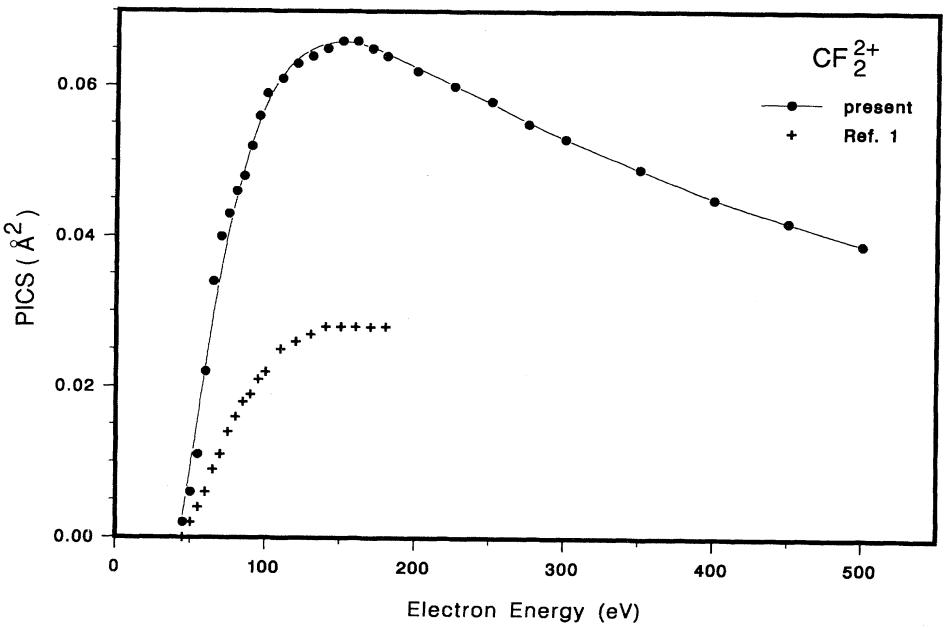

FIG. 16. Absolute partial ionization cross sections of CF_2^{2+}. Dots: present work; pluses: Ref. [1].

much as 26% higher than Stephan *et al.* [1]. This situation holds true for all the absolute partial ionization cross sections (CF_3^+, CF_2^+, CF_3^{2+}, CF^+, CF_2^{2+}, F^+, and C^+) as shown in Figs. 12–18. Among all the ion fragments, the difference is the smallest for CF_3^+ with our results 9% larger at 80 eV, well within the stated uncertainties. However, the discrepancies become much larger for the lighter-ion fragments which are believed to possess higher dissociative kinetic energies.

Märk has pointed out the existence of a recent paper from his laboratory [22] in which the problem of detecting ions with high translational kinetic energies is ad-

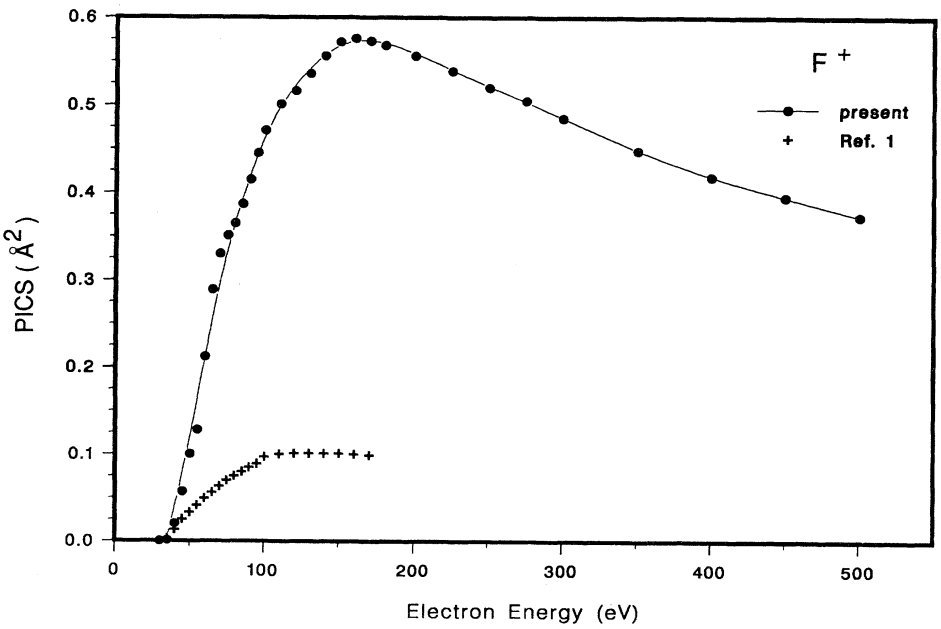

FIG. 17. Absolute partial ionization cross sections of F^+. Dots: present work; pluses: Ref. [1].

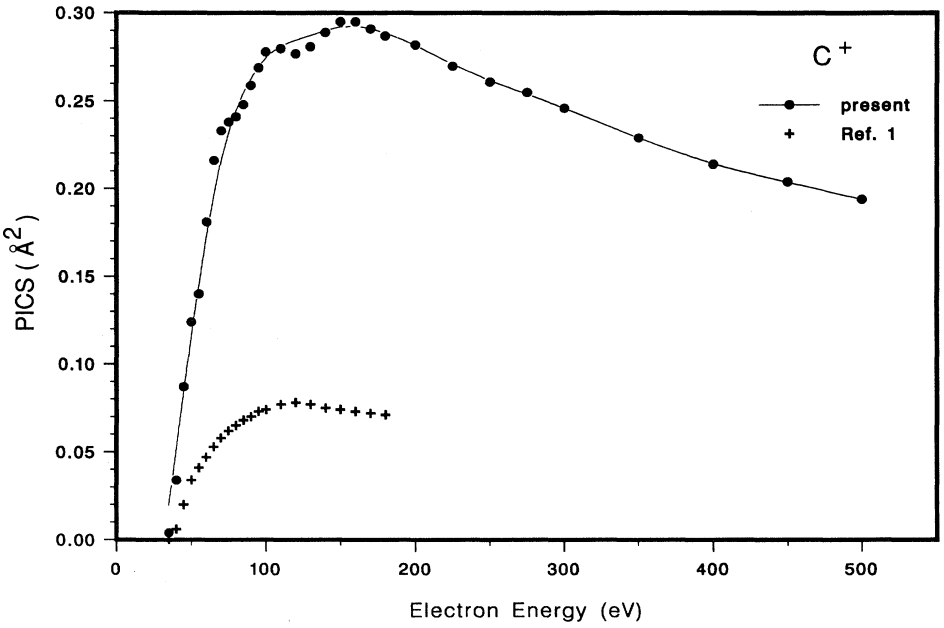

FIG. 18. Absolute partial ionization cross sections of C^+. Dots: present work; pluses: Ref. [1].

dressed. This paper outlines methods for correcting data such as that given in Ref. [1] and Märk has been kind enough to send us his corrected data on CF_4 in advance of publication. In Table II, the results from Ref. [1], uncorrected for ion translational energy, can be compared with the corrected values, the values from this study, and photoionization results obtained from an electron-ion coincidence experiment [23]. All results were obtained at 80 eV or its equivalent photon energy. It should be noted that the relative abundances of singly charged ions as obtained by the corrected results of Ref. [1] and from our work are in excellent agreement.

Because the determination of the absolute scale is a separate problem from determination of the ion ratios in both of our experimental methods, it appears best to discuss the agreement between our results and the new results communicated to us by Märk in terms of these two separate issues. The absolute scale agreement was determined by computing the ratio of CF_3^+ cross sections at 25, 50, 75, 100, 120, 150, and 180 eV. Our results are lower on average by 22±3%. The small value of the standard deviation indicates that the energy dependencies (shapes) of the two cross-section sets are in excellent agreement. Although the 22% difference between the two scales is within the uncertainties claimed by the two groups, it is worth noting that our initial estimates of the absolute scale based on expanding a mixture of Ar, Kr, and CF_4 of known concentration and normalizing the CF_3^+ absolute scale to the Rapp Englander-Golden values for Ar and Kr yielded results in excellent agreement with the current values furnished to us by Märk. We had abandoned this approach because of a worry that the distributions of the different gases emanating from the nozzle could be different and because of time-dependent variations in observed ion ratios. A further consideration was the fact that the total dissociative ionization cross section exceeded the total dissociation cross section reported by Winters and Inokuti. The resolution of this problem will have to wait further experimental work.

We have determined the cross-section ratios $\sigma_{CF_2^+}/\sigma_{CF_3^+}$, $\sigma_{CF^+}/\sigma_{CF_3^+}$, $\sigma_{F^+}/\sigma_{CF_3^+}$, $\sigma_{C^+}/\sigma_{CF_3^+}$, $\sigma_{CF_3^{2+}}/\sigma_{CF_3^+}$, and $\sigma_{CF_2^{2+}}/\sigma_{CF_3^+}$ at 50, 75, 100, 130, and 180 eV for the two sets of measurements. The $\sigma_{CF_2^+}/\sigma_{CF_3^+}$ ratio shows an average agreement of 5% with a maximum deviation of 10%. Our ratio values are larger in each case except at 50 eV. For $\sigma_{CF^+}/\sigma_{CF_3^+}$, the average agreement is 3% with a maximum deviation of 7% and all our values are larger. In the case of $\sigma_{F^+}/\sigma_{CF_3^+}$, the average agreement, excluding the point at 40 eV, is 6% with a maximum deviation of 12%. The

TABLE II. Percentages of the number of fragment ions at 80-eV electron energy (Ref. [1], Ref. [1] corrected for translational kinetic-energy effects, and present) and photon energy (Ref. [22]).

Ion	SDM (Ref. [1])	SDM (corrected)	Present	Photon impact (Ref. [23])
CF_3^+	86.0	70.6	70.6	67.3
CF_2^+	6.1	6.7	6.9	6.4
CF_3^{2+}	0.2	0.1	0.5	
CF^+	3.2	7.5	7.4	6.5
CF_2^{2+}	0.5	0.3	1.0	1.1
F^+	2.1	9.2	8.1	12.5
C^+	1.9	5.0	5.4	6.2

point at 50 eV deviates by 40% and all our ratios are *smaller*. For $\sigma_{CF^+}/\sigma_{CF_3^+}$, the average agreement is 10% with a maximum deviation of 15% and all our values are larger. The ratios involving the doubly charged species are three to six times larger in our measurements for $\sigma_{CF_3^{2+}}/\sigma_{CF_3^+}$ and two to three times larger for $\sigma_{CF_2^{2+}}/\sigma_{CF_3^+}$ with monotonic variation in incident energy and with the smaller factor at the highest energy.

In summary, the agreement between our results and the corrected results of Ref. [1] for singly charged ions are all within the $\pm 15\%$ uncertainty assigned to each experiment. The serious disagreement encountered with the doubly charged species was also observed in earlier studies on Ar [4]. We have checked the $\sigma(Ar^{2+}/Ar^+)$ cross-section ratio as a function of the impact energy on the front of our microchannel plate detector and find it to be constant from 2 to 4 keV Ar^+ translational kinetic energy (4–8 keV for Ar^{2+}), which rules out a differing detector efficiency as the cause of the difference. This would appear to suggest that the discrepancy arises in either the ion production or ion transport regions in one or both of the two experiments. However, the small cross sections of the doubly charged species makes it unlikely that any serious difference will occur in technological applications such as plasma modeling using either cross-section data base. Experiments in our laboratory are currently underway to explore possible reasons for the multicharged species problem.

Finally, it is worth noting that a new semiempirical theory for calculating total ionization cross sections [24] for molecules has been published which has been very successful in fitting experimental results. The predictions of this theory are in excellent agreement with our results for the total ionization cross section.

ACKNOWLEDGMENTS

The authors wish to thank the National Science Foundation for Grant No. NSF PHY-8913096, which made this work possible. We owe Professor T. Märk a debt of gratitude for his helpful suggestions and for sharing his latest results with us in advance of publication. We also wish to thank the Chemistry Department's Electronic, Computer and Mechanical Instruments service groups for their help in the design and construction of the apparatus.

[1] K. Stephan, H. Deutsch, and T. Märk, J. Chem. Phys. **83**, 5712 (1985).
[2] V. N. Slavik, N. N. Chavarga, P. V. Fel'tsan, and I. S. Aleksakhin, Zh. Tekh. Fiz. **57**, 2409 (1987) [Sov. Phys. Tech. Phys. **32**, 1463 (1987)].
[3] H. F. Winters and M. Inokuti, Phys. Rev. A **3**, 1420 (1982).
[4] Ce Ma, C. R. Sporleder, and R. A. Bonham, Rev. Sci. Instrum. **62**, 909 (1991).
[5] Ce Ma, P. B. Liescheski, and R. A. Bonham, Rev. Sci. Instrum. **60**, 3661 (1989).
[6] D. A. Dahl and J. E. Delmore, The SIMION PC/AT User's Manual, Vol. 3.0, Idaho National Engineering Laboratory, Report No. EGG-CS-7233, 1987.
[7] R. S. Gao, P. S. Gibner, J. H. Newman, K. A. Smith, and R. F. Stebbings, Rev. Sci. Instrum. **55**, 1756 (1984).
[8] A. Müller, N. Djurić, G. H. Dunn and D. S. Belić, Rev. Sci. Instrum. **57**, 349 (1986).
[9] K. Tobita, H. Takeuchi, H. Kimura, Y. Kusama, and M. Nemoto, Jpn. J. Appl. Phys. **26**, 509 (1987).
[10] B. Brehm, R. Frey, A. Kustler, and J. H. D. Eland, Int. J. Mass Spectros. Ion Phys. **13**, 251 (1974).
[11] H. A. Van Sprang, H. H. Brongersma, and F. J. De Heer, Chem. Phys. **35**, 51 (1978).
[12] J. F. M. Aarts, Chem. Phys. Lett. **114**, 114 (1985).
[13] K. A. Blanks and K. Becker, J. Phys. B **20**, 6157 (1987).
[14] K. Becker (private communication).
[15] S. Wang, J. L. Forand, and J. W. McConkey, Can. J. Phys. **67**, 699 (1989).
[16] U. Fano, Phys. Rev. **95**, 1198 (1954).
[17] R. Jones (unpublished).
[18] R. A. Bonham and M. Fink, *High Energy Electron Scattering* (Van Nostrand Reinhold, New York, 1974) ACS monograph No. 169.
[19] M. Fink (private communication).
[20] T. Sakae, S. Sumiyoshi, E. Murakami, Y. Matsumoto, K. Ishibashi, and A. Katase, J. Phys. B **22**, 1385 (1989).
[21] P. Bromberg (unpublished).
[22] D. Margrreiter, G. Walder, H. Deutsch, H. U. Poll, C. Winkler, K. Stephan, and T. D. Märk, Int. J. Mass Spectros. Ion Proc. **100**, 143 (1990).
[23] W. Zhang, G. Cooper, T. Ibuki, and C. E. Brion, Chem. Phys. **137**, 391 (1989).
[24] D. Margreiter, H. Deutsch, M. Schmidt, and T. D. Märk, Int. J. Mass Spectros. Ion Proc. **100**, 157 (1990).